



Universiteit
Leiden
The Netherlands

Determinants of genome editing outcomes: the impact of target and donor DNA structures

Chen, X.

Citation

Chen, X. (2018, May 16). *Determinants of genome editing outcomes: the impact of target and donor DNA structures*. Retrieved from <https://hdl.handle.net/1887/62204>

Version: Not Applicable (or Unknown)

License: [Licence agreement concerning inclusion of doctoral thesis in the Institutional Repository of the University of Leiden](#)

Downloaded from: <https://hdl.handle.net/1887/62204>

Note: To cite this publication please use the final published version (if applicable).

Cover Page



Universiteit Leiden



The following handle holds various files of this Leiden University dissertation:

<http://hdl.handle.net/1887/62204>

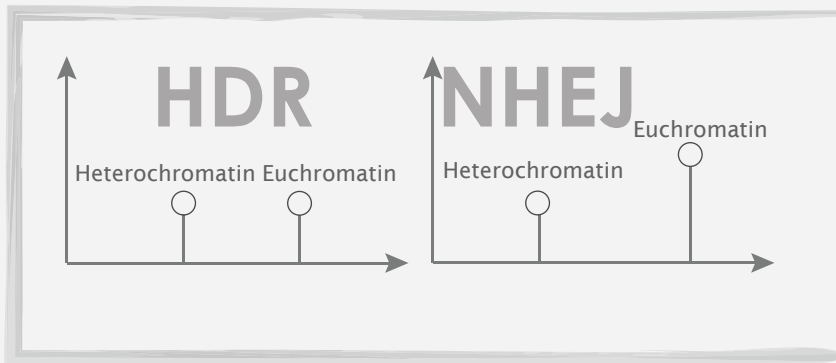
Author: Chen, X.

Title: Determinants of genome editing outcomes: the impact of target and donor DNA structures

Issue Date: 2018-05-16

Chapter 5

The **Chromatin** Structure **Governs** Gene-editing Outcomes



Josephine M. Janssen*, Xiaoyu Chen*, Jin Liu and Manuel A.F.V.
Gonçalves

*Co-first Authors

Abstract

Gene editing based on homology-directed repair (HDR) depends on donor DNA and sequence-specific programmable nucleases. However, in addition to inducing HDR involving the mending of chromosomal double-stranded breaks (DSBs) with donor DNA templates, programmable nucleases also yield gene disruptions by triggering the competing non-homologous end-joining (NHEJ) pathway. Hence, it is crucial to identify parameters underlying the choice between these two DNA repair pathways in the context of HDR-based gene editing. Here, we implemented quantitative cellular systems based on epigenetically regulated isogenic target sequences and donor DNA of viral, non-viral and synthetic origins, to investigate gene editing outcomes resulting from the interaction between different chromatin conformations and donor DNA structures. We demonstrate that the chromatin topology influences gene editing endpoints by shifting the balance between HDR and NHEJ events. In particular, HDR increases in relation to NHEJ when chromosomal target sequences acquire a heterochromatic state. Moreover, albeit varying in degree, this shift in the balance between HDR- and NHEJ-induced chromosomal changes (1.5- to 6.4-fold) takes place independently of the types of episomal donor DNA. Besides establishing a direct relationship between specific gene editing outcomes and epigenetically regulated higher-order chromatin “conformers”, these findings might guide the development of improved genome engineering procedures.

Introduction

Genome editing based on inducing targeted chromosomal double-stranded DNA breaks (DSBs) by programmable nucleases permits altering, in a precise manner, the genetic make-up of eukaryotic cells.^{1,2} Normally, homology-directed repair (HDR) is the DSB repair pathway that participates in the targeted addition of new genetic information. In this case, exogenous DNA templates sharing sequences identical to chromosomal acceptor sites serve as surrogate HDR substrates for repairing the underlying sequence-specific DSBs. Ultimately, this co-option of HDR yields precise genetic alterations at predefined genomic sequences.^{1,2}

Despite its patent usefulness, HDR-based gene editing is limited by the fact that, in mammalian cells, DSBs are primarily repaired through competing non-homologous end-joining (NHEJ) pathways instead of through HDR.^{3,4} Moreover, HDR is commonly restricted to the mitotic G2/S phases of the cell cycle, when allelic sister chromatid sequences become available, while NHEJ, involving simply end-to-end ligation of broken chromosomal termini, takes place throughout the various stages of the cell cycle.^{3,4} Critically, NHEJ-mediated DSB repair often leads to the incorporation of small insertions and deletions (indels) at the target site resulting in disruptive and potentially deleterious byproducts, e.g., chromosomal translocations

and/or allelic mutations. Hence, it is important to expand our knowledge about the parameters governing the choice between these two major DNA repair pathways which, together, determine the performance of HDR-based gene editing and genomic DNA stability.

Chromatin is formed in the nucleus of eukaryotic cells by a dynamic association between genomic DNA and various types of molecules, including, histones and non-histone proteins. The basic unit of chromatin, the nucleosome, consists of ~ 147 bps of double helix wrapped around an octamer of the four core histones H3, H4, H2A and H2B.⁵ The transition from compact, or “closed”, heterochromatin to relaxed, or “open”, euchromatin is controlled through a large number of macromolecular complexes and their respective catalytic activities, which include methylation-demethylation, acetylation-deacetylation and phosphorylation-dephosphorylation.⁵ Recently, our laboratory and that of others reported that NHEJ-mediated repair of single DSBs induced by programmable nucleases can be modulated by distinct chromatin structures.^{6,7} As of yet, however, the role played by such 3D structures on the performance of HDR-based gene editing has not been assessed. To address this matter, here, we sought to specifically investigate whether distinct higher-order chromatin conformations control gene editing outcomes by changing the balance between HDR and NHEJ at single, site-specific, DSBs. For these experiments, we combined programmable RNA-guided nucleases (RGN) based on the type II clustered regularly interspaced short palindromic repeats (CRISPR)-Cas9 adaptive immune system from *S. pyogenes*,⁸ with donor HDR substrates of viral, non-viral and synthetic origins. In particular, as donors, we tested integrase-defective lentiviral vector genomes (IDLVs),⁹ conventional recombinant plasmids and chemically synthesized single-stranded oligodeoxyribonucleotides (ODNs) with both polarities. RGNs are ribonucleoproteins formed by a complex between a fixed Cas9 protein and a flexible guide RNA (gRNA). Typically, the 5'-terminal 20 nucleotides of the gRNA (spacer) are tailored to hybridize to a chromosomal target sequence located next to a protospacer adjacent motif (PAM; NGG in the case of *S. pyogenes* Cas9). The PAM sequence signals the position for the initial protein-DNA binding mediated through the PAM-interacting domain positioned on two lobes of Cas9.¹⁰ Next, complementarity between the spacer portion of the gRNA and PAM-adjacent DNA sequences triggers DSB formation by the coordinated catalytic activation of the nuclease domains of Cas9 (i.e. HNH and RuvC).⁸

By using the aforementioned DNA, RNA and protein tools, we performed gene-editing experiments in quantitative live-cell readout systems based on human reporter cells containing chromosomal target sequences whose epigenetic statuses are controlled by small molecule drug availability.⁶ We report that the proportions between gene editing endpoints resulting from the repair of site-specific DSBs by NHEJ and HDR differ in a chromatin structure-dependent manner with HDR increasing its



HDR
during
hetero
DSB
repair

prominence in relation to NHEJ when target sequences transit from an euchromatic to an heterochromatic state.

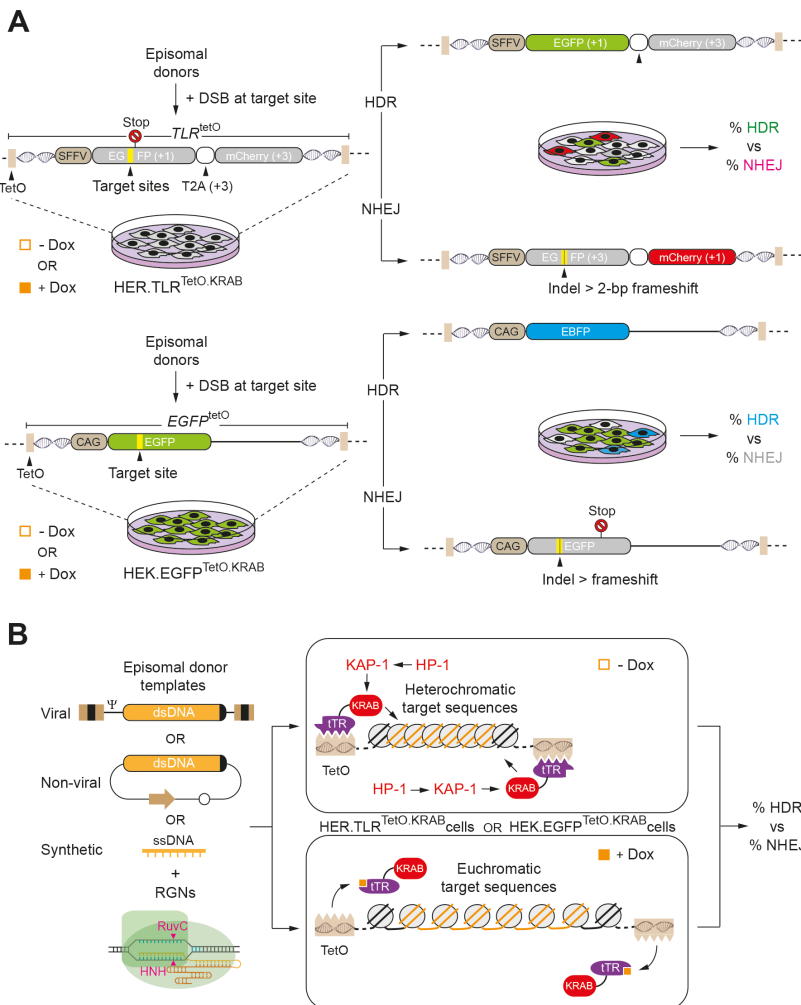
Results

Gene editing experiments were carried out in HER.TLR^{TetO.KRAB} and HEK.EGFP^{TetO.KRAB} cells (**Figure 1A**). These human reporter cells express the *E. coli* tetracycline trans-repressor (tTR) fused to a mammalian Krüppel-associated box domain (KRAB). The tTR and KRAB components are the DNA-binding and effector domains of the tTR-KRAB fusion product, respectively. KRAB-containing proteins belong to the largest family of zinc-finger repressors in tetrapod vertebrates whose generic role is to recruit chromatin remodeling co-repressors via their KRAB domains after binding to specific genomic sequences through their zinc-finger motifs.¹⁵ In particular, KRAB domains interact with KRAB-associated protein 1 (KAP-1) oligomers that form a scaffold for the binding of heterochromatin protein 1 (HP-1) isoforms (i.e. HP1 α , HP1 β and HP1 γ), histone deacetylases (i.e. HDAC1 and HDAC2), the nucleosome remodeling factor CHD3 and the SET-domain histone methyl-transferase SETDB1 that lead to the recruitment of additional HP1 molecules via tri-methylation of lysine 9 on histone H3 (H3K9me3).¹⁶ Ultimately, these large protein-DNA assemblies create heterochromatic regions in the genome.¹⁷ In HER.TLR^{TetO.KRAB} and HEK.EGFP^{TetO.KRAB} cells, in the absence of Dox, the tTR-KRAB fusion protein binds to its cognate *TetO* sequences and recruits via its KRAB repressor domain the endogenous epigenetic silencing apparatus involving, amongst other chromatin remodeling factors, KAP-1 and HP-1 (**Figure 1B**). Conversely, in the presence of Dox, tTR-KRAB suffers a conformational change that releases it from the *TetO* sequences, resulting in the transition of associated sequences from a compacted heterochromatic state (H3K9me3 high; H3-Ac low) into a relaxed euchromatic state (H3-Ac high; H3K9me3 low).⁶

We reasoned that the complementary gain-of-function and loss-of-function assays offered by HER.TLR^{TetO.KRAB} and HEK.EGFP^{TetO.KRAB} cells should be particularly suited for assessing the impact of epigenetically regulated chromatin conformations on specific gene editing endpoints. This is so owing to the fact that these live-cell systems permit the simultaneous quantification of HDR and NHEJ events at isogenic target sequences located either in euchromatin or heterochromatin depending on the presence or absence of Dox, respectively (**Figure 1B**). Indeed, in these cells, Dox availability regulates the tTR-KRAB-mediated recruitment of the aforementioned endogenous chromatin remodeling complexes to *TetO* sequences associated with each of the reporter alleles, i.e., *TLR^{TetO}* and *EGFP^{TetO}* (**Figure 1A**).

HDR-based gene editing experiments were started by transfecting HER.TLR^{TetO.KRAB} cells, cultured in the absence or in the presence of Dox, with expression plasmids encoding the RGN complex Cas9:gTLR.1 (**Supplementary Figure S1**). The target site

of Cas9:gTLR.1 is located upstream of a nonsense mutation within the TLR^{TetO} construct (**Figure 1A** and **Supplementary Figure S2**) and is flanked by sequences “homologous” to those present in the *EGFP*-repairing donor template *EGFPtrunc*.¹² This HDR substrate was delivered by transducing HER.TLR^{TetO,KRAB} cells with different amounts of the integrase-defective lentiviral vector IDLV^d together with constructs expressing the RGN complex Cas9:gTLR.1 (**Figure 1B**). Negative controls were provided by HER.TLR^{TetO,KRAB} cells that were neither transfected with expression plasmids nor transduced with IDLV^d particles (Mock) and by HER.TLR^{TetO,KRAB} cells that were exposed to an irrelevant, non-targeting, gRNA (gNT) together with Cas9 and IDLV^d. After the action of the RGN complexes had taken place, all HER.TLR^{TetO,KRAB} cultures were incubated in the presence of Dox for allowing transgene expression and quantification of HDR and NHEJ events by EGFP- and mCherry-directed flow cytometry respectively (**Figure 1A** and **Supplementary Figure S1**).



HDR
during
hetero-
DSB
repair

Figure 1. Experimental systems for tracking gene editing outcomes at isogenic target sequences with alternative higher-order epigenetic states. **(A)** *Modus operandi* of the cellular systems for tracking gene-editing endpoints at heterochromatin versus euchromatin. Upper panel, the *TetO*-flanked *TLR^{TetO}* construct in tTR-KRAB-expressing HER.TLR^{TetO.KRAB} cells has an *EGFP* ORF interrupted by heterologous sequences and a stop codon located upstream of a *T2A* sequence and an out-of-frame *mCherry* reporter. HDR is scored by measuring EGFP+ cells resulting from the repair of site-specific DSBs by HR events between episomal donor templates (*EGFPtrunc*) and heterochromatic (-Dox) or euchromatic (+Dox) chromosomal DNA. This genetic exchange results in the substitution of the heterologous and stop codon DNA by an in-frame EGFP sequence. Concomitantly, NHEJ is scored by measuring mCherry+ cells resulting from indels placing the mCherry in-frame. Lower pane, the *TetO*-flanked *EGFP* construct (*EGFP^{TetO}*) in tTR-KRAB-expressing HEK.EGFP^{TetO.KRAB} cells is functional. HDR is tracked by measuring the frequencies of blue light-emitting cells resulting from the conversion of the EGFP fluorochrome to that of EBFP. Simultaneously, NHEJ is scored by measuring EGFP- cells resulting from indels placing the *EGFP* sequence out-of-frame. **(B)** Generic experimental designs. The reporter HER.TLR^{TetO.KRAB} and HEK.EGFP^{TetO.KRAB} cells, cultured in the absence or in the presence of Dox, are exposed to RGNs together with different donor DNA templates. Without Dox, tTR-KRAB binds to *TetO* and induces heterochromatin formation through the recruitment of, amongst others, KAP-1 and HP-1. With Dox, tTR-KRAB set free *TetO* leading the target sequences to acquire an euchromatic state. After the completion of the gene editing processes, Dox is added to the different cultures in order to determine the frequencies of HDR and NHEJ events at heterochromatic versus euchromatic target sequences by dual-color flow cytometry.

The results obtained from this experiment revealed that the frequencies of DSB-triggered NHEJ at euchromatic target sequences (+Dox) were substantially higher than those measured at their heterochromatic (-Dox) counterparts as assessed by mCherry-directed flow cytometry (**Figures 2A** and **2B**). This outcome is in agreement with that of our previous study involving the exclusive delivery of RGNs into HER.TLR^{TetO.KRAB} cells.⁶ In particular, RGN-induced DSBs are preferentially formed at euchromatin over heterochromatin,⁶ which, in turn, correlates with the preferential binding of RGNs harboring catalytically inert (“dead”) Cas9 proteins to euchromatic over heterochromatic regions across the genome.¹⁸⁻²⁰ Interestingly, despite of the initial higher accessibility of gene editing tools to euchromatic over heterochromatic genomic DNA, there were no corresponding increases in HDR levels in the former, Dox-treated, cells (**Figures 2A** and **2B**). As a result, the ratios between NHEJ and HDR events at compact heterochromatin were substantially lower than those measured at relaxed euchromatin (4.6- to 5.3-fold), regardless of the amounts of exogenous HDR templates available for recombination (**Figure 2C**, top graph). This outcome translated in a relative increase in HDR (+) and a decrease in NHEJ (-) at heterochromatin (**Figure 2C**, bottom graph). The use of the alternative RGN complex Cas9:gTLR.2 (**Figure 3A** and **Supplementary Figure S3**) and a different transfection protocol (**Figures 3B** and **3C**), led to similar NHEJ/HDR ratios and variations in the frequencies of HDR and NHEJ (compare **Figure 3D** with **Figure 2C**, respectively).

Next, we sought to determine RGN-induced gene editing endpoints at isogenic target sequences with distinct higher-order chromatin conformations after delivering donor DNA in the context of covalently closed double-stranded plasmids. In these

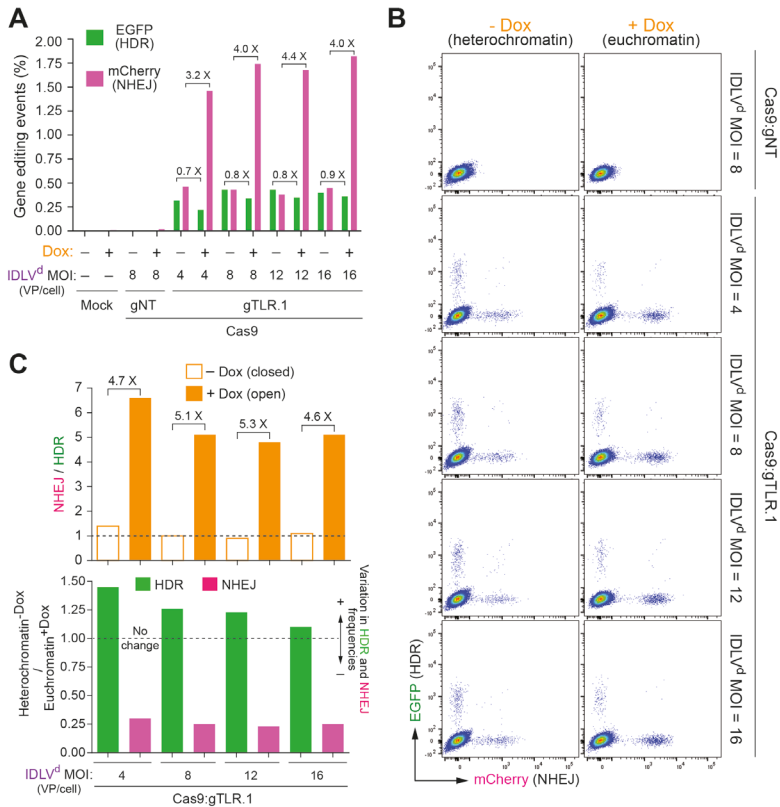


Figure 2. Gene editing endpoints at euchromatin versus heterochromatin after IDLV donor DNA delivery. **(A)** Dual-color flow cytometric quantification of HDR and NHEJ events in HER.TLR^{TetO,KRAB} cells. HER.TLR^{TetO,KRAB} cells were exposed to Cas9:gTLR.1 together with the indicated multiplicities of infection (MOI) of IDLV^d. Negative controls consisted of mock-treated cultures and of cultures exposed to a non-targeting gRNA (gNT), Cas9 and IDLV^d at an MOI of 8 vector particles per cell (VP/cell). The various experimental conditions were tested in HER.TLR^{TetO,KRAB} reporter cells incubated in the absence (-) or in the presence (+) of doxycycline (Dox). The frequencies of HDR and NHEJ events in the various target cell populations were determined by measuring EGFP+ and mCherry+ cells, respectively. **(B)** Dot plots corresponding to HER.TLR^{TetO,KRAB} cells transduced with different doses of IDLV^d particles and subjected to the indicated Dox regimens. **(C)** Relative participation of HDR and NHEJ pathways during IDLV-mediated repair of DSBs occurring at heterochromatin versus euchromatin. In the top graph, data of panel **A** are presented as the ratios between the frequencies of NHEJ and HDR in HER.TLR^{TetO,KRAB} cells not treated and treated with Dox (top graph). In the bottom graph, data of panel **A** are depicted as the variation in the proportion of HDR and NHEJ events at heterochromatin versus euchromatin.

experiments, we deployed the lentiviral DNA construct Plasmid^d,¹² which had been utilized for assembling IDLV^d particles. Again, these gene editing experiments involved the use of two different transfection protocols for introducing donor Plasmid^d mixed with constructs expressing either Cas9:gTLR.1 or Cas9:gTLR.2 complexes into HER.TLR^{TetO,KRAB} cells treated or not treated with Dox (**Figures 3E-G**). The resulting gene editing outcomes (**Figures 3E-H**) were similar to those obtained after



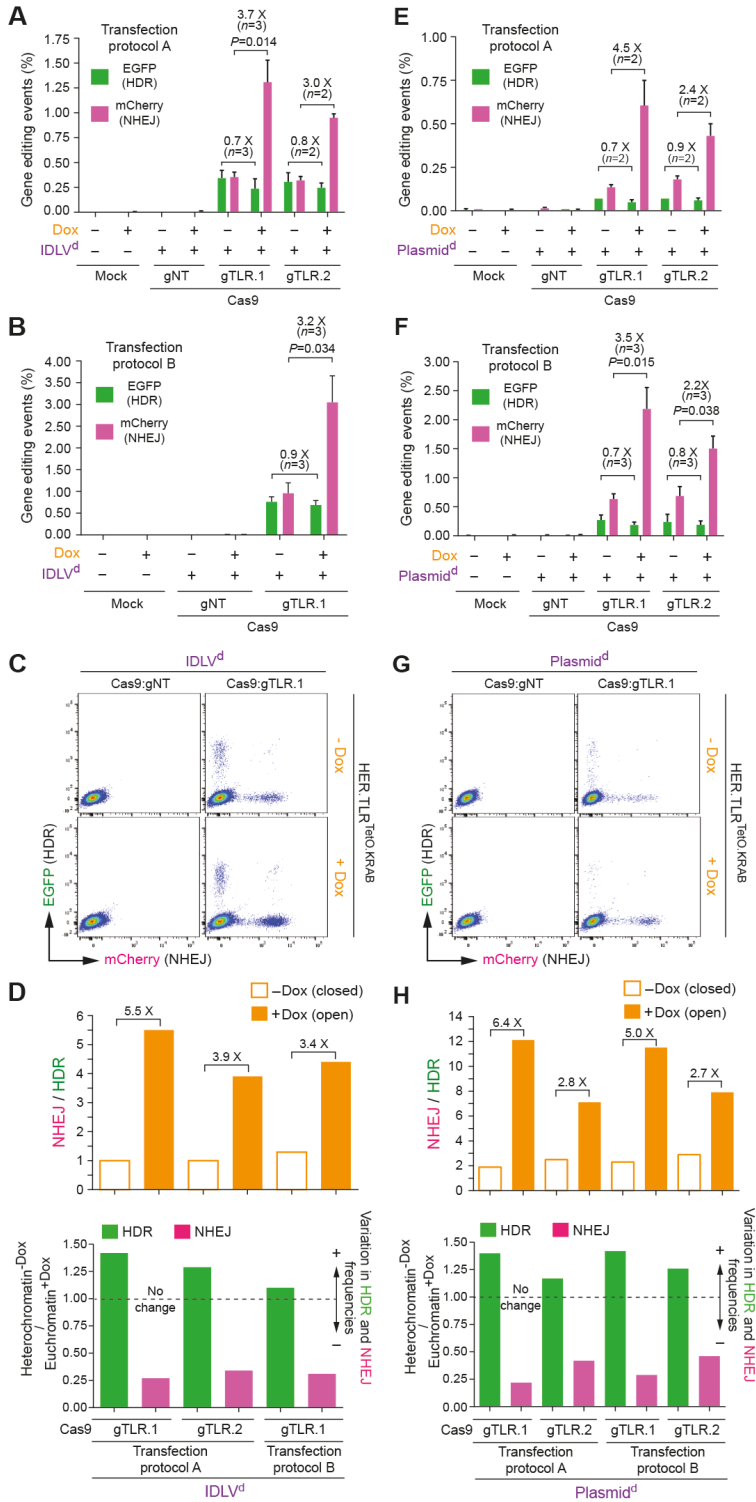


Figure 3. Comparing gene editing outcomes at euchromatin versus heterochromatin after viral and plasmid vector delivery of donor DNA. (**A** and **B**) IDLV^d-based gene editing. Dual-color flow cytometric measurements of HDR and NHEJ frequencies in HER.TLR^{TetO.KRAB} cells subjected to the indicated experimental conditions and treated (+) or not treated (-) with Dox. Two different transfection protocols (**A** and **B**) were used to introduce the DNA constructs into target cells. IDLV^d particles were applied at an MOI of 8 VP/cell. (**C**) Representative dot plots corresponding to HER.TLR^{TetO.KRAB} cells exposed to IDLV^d together with Cas9:gNT or Cas9:gTLR.1 complexes. (**D**) Comparative engagement of HDR and NHEJ pathways during IDLV-mediated repair of DSBs made at heterochromatin versus euchromatin. Top graph, data of panels **A** and **B** presented as the ratios between the rates of NHEJ and HDR in HER.TLR^{TetO.KRAB} cells either incubated or not incubated with Dox. Bottom graph, data of panels **A** and **B** depicted as the variation in the fraction of HDR and NHEJ events at heterochromatin versus euchromatin. (**E** and **F**) Plasmid^d-based gene editing. Dual-color flow cytometric quantification of HDR and NHEJ frequencies in HER.TLR^{TetO.KRAB} cells. HER.TLR^{TetO.KRAB} cells incubated (+) or not incubated (-) with Dox, were either mock-transfected or were transfected with Plasmid^d mixed with constructs encoding the indicated RGN complexes. Two different transfection protocols (**A** and **B**) were used to deliver the DNA constructs into target cells. (**G**) Representative dot plots corresponding to HER.TLR^{TetO.KRAB} cells transfected with Plasmid^d mixed with expression constructs coding for Cas9:gNT or Cas9:TLR.1 complexes. (**H**) Relative engagement of HDR and NHEJ pathways during plasmid-mediated repair of DSBs created at heterochromatin versus euchromatin. Top graph, results of panels **E** and **F** depicted as ratios between the frequencies of NHEJ and HDR in HER.TLR^{TetO.KRAB} cells exposed or not exposed to Dox. Bottom graph, data of panels **E** and **F** shown as the variation in HDR and NHEJ events at heterochromatin versus euchromatin. Bars in graphs **A**, **B**, **E** and **F** correspond to mean \pm s.d. of the indicated number (*n*) of independent experiments (biological replicates done in different days).

IDLV^d transduction of HER.TLR^{TetO.KRAB} cells (**Figure 2** and **Figures 3A-D**). In particular, in comparison with euchromatin, at heterochromatin, the balance between NHEJ and HDR shifts towards the latter pathway causing target cell populations to acquire a more even distribution between HDR- and NHEJ-derived genetic modifications (**Figure 3H**).

To serve as additional controls, gene editing experiments were also performed in tTR-KRAB-expressing HER.TLR^{KRAB} cells whose target sequences are not under conditional KRAB-mediated epigenetic regulation due to their lack of *TetO cis*-acting elements necessary for tTR-KRAB binding (**Figure 4A**). Importantly, regardless of the Dox regiment, neither the HDR levels nor the NHEJ levels changed in HER.TLR^{KRAB} cells, independently of whether the donor DNA was introduced into target cell nuclei in the context of linear IDLV^d genomes (**Figures 4B** and **4C**) or covalently closed Plasmid^d molecules (**Figures 4D** and **4E**). Hence, in contrast with gene editing experiments in HER.TLR^{TetO.KRAB} cells, in control HER.TLR^{KRAB} cells, there were no substantial Dox-dependent variations in the proportions between HDR and NHEJ events for both types of donor DNA templates used (**Figure 4F**).

Next, we performed gene-editing experiments in HEK.EGFP^{TetO.KRAB} cells. In this independent experimental system, HDR can be promptly tracked by measuring cells in which the EGFP fluorochrome is converted into that of EBFP, while NHEJ can be monitored through quantifying cells with indel-derived EGFP knockouts (**Figures**

HDR
during
hetero
DSB
repair

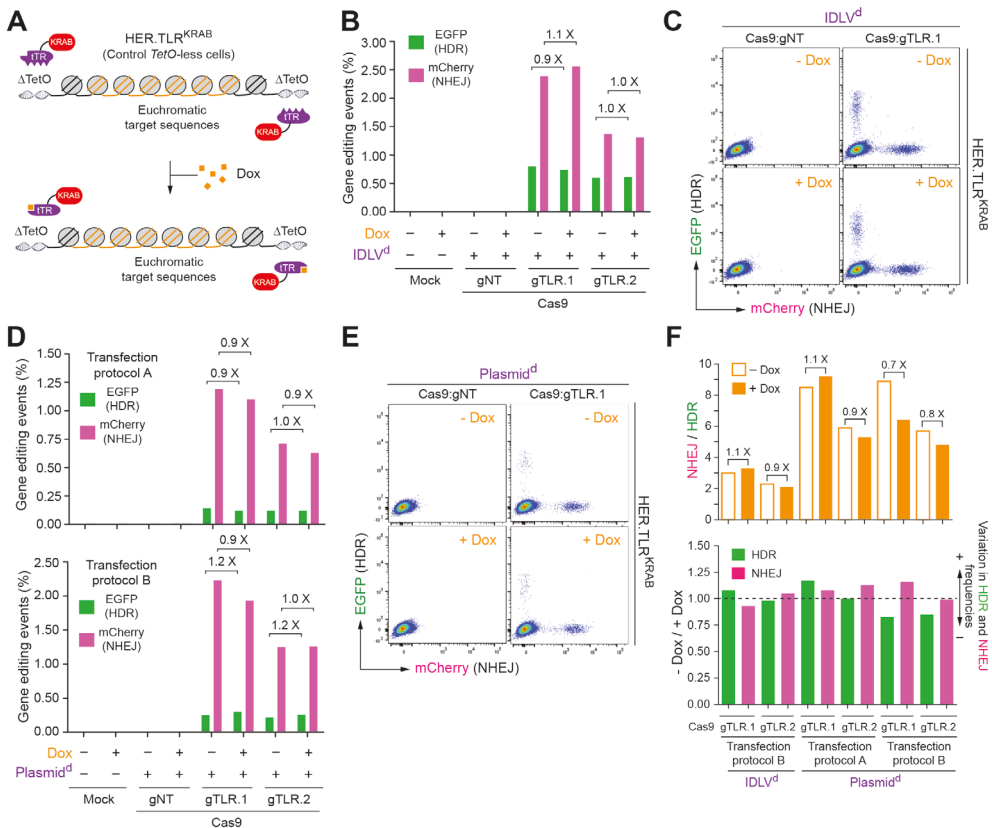


Figure 4. Gene editing endpoints in control HER.TLR^{KRAB} cells exposed or not exposed to Dox. **(A)** Schematics of target DNA in HER.TLR^{KRAB} cells. The tTR-KRAB-expressing HER.TLR^{KRAB} cells have a Dox-insensitive *TLR* construct due to its lack of *cis*-acting *TetO* elements. **(B)** Dual-color flow cytometric quantification of HDR and NHEJ events in HER.TLR^{KRAB} cells. HER.TLR^{KRAB} cells, treated (+) or not treated (-) with Dox, were exposed to the indicated experimental conditions. IDLV^d particles were applied at an MOI of 8 VP/cell. **(C)** Representative dot plots corresponding to HER.TLR^{KRAB} cells exposed to IDLV^d particles together with Cas9:gNT or Cas9:TLR.1 complexes. **(D)** Dual-color flow cytometric quantification of HDR and NHEJ frequencies in HER.TLR^{KRAB} cells. HER.TLR^{KRAB} cells, incubated (+) or not incubated (-) with Dox, were mock transfected or were transfected with plasmid mixed with constructs encoding the indicated RGN complexes. Two different transfection protocols (A and B) were used to deliver the DNA constructs into target cells. **(E)** Dot plots corresponding to HER.TLR^{KRAB} cells transfected with Plasmid^d mixed with expression constructs coding for Cas9:gNT or Cas9:TLR.1 complexes. **(F)** Comparative engagement of HDR and NHEJ pathways at site-specific DSBs created at heterochromatin versus euchromatin. Top graph, data of panels **B** and **D** presented as ratios between the rates of NHEJ and HDR in HER.TLR^{KRAB} cells not incubated or incubated in the presence of Dox. Bottom graph, data of panels **B** and **D** shown as the variation in the fraction of HDR and NHEJ events at heterochromatin versus euchromatin.

DSB induced by Cas9:gRNA^{EGFP}. **(B)** Schematics of the experimental design applied to HEK. EGFP^{TetO.KRAB} cells. **(C)** Flow cytometric quantification of HDR and NHEJ frequencies. HEK. EGFP^{TetO.KRAB} cells, incubated (+) or not incubated (-) with Dox, were exposed to pTHG.Donor and gRNA^{EGFP}-containing RGNs. The frequencies of HDR and NHEJ events in the transfected cell populations were determined by measuring EBFP+ and EGFP- cells, respectively. A minimum of forty thousand events, each corresponding to a single viable cell, were acquired per sample. **(D)** Relative participation of HDR and NHEJ pathways during plasmid-mediated repair of DSBs made at heterochromatin versus euchromatin. Top graph, data of panel **C** presented as the ratios between the frequencies of NHEJ and HDR in HEK.EGFP^{TetO.KRAB} cells treated and not treated with Dox. Bottom graph, data of panel **C** depicted as the variation in the proportion of HDR and NHEJ events at heterochromatin versus euchromatin.

Finally, to complement the previous experiments testing linear and covalently closed double-stranded donors in the form of IDLV genomes and recombinant plasmids, respectively, we sought to assess ODN-based gene editing at euchromatin versus heterochromatin. For these experiments, we selected a single-stranded ODN pair corresponding to the sense and antisense polarities of the target polynucleotide chains of Cas9:gEGFP (i.e. ODN.s and ODN.as, respectively). Previous research has demonstrated that RGNs can display a long residence time on target DNA (~ 6 h) and that, after DNA cutting, the strand upstream of the PAM (non-target strand) is released from the Cas9-gRNA-DNA ternary complex forming a 3'-ended DNA flap (**Figure 6A**).²¹ This insight permitted the design of optimized single-stranded ODN donors which are complementary to the released strand. Indeed, when compared to double-stranded and single-stranded ODNs that cannot anneal to RGN-generated flaps, ODNs complementary to the released strand induced ~ 4- and ~ 2-fold higher frequencies of HDR in human cells, respectively.²¹ Results from an initial experiment in HEK.EGFP^{TetO.KRAB} cells exposed to Cas9:gEGFP together with ODN.s or with ODN.as were consistent with the aforementioned data in that the ODN.as yielded ~2-fold higher frequencies of HDR than the ODN.s (**Figure 6B**). Interestingly, expanding these ODN transfection experiments to HEK.EGFP^{TetO.KRAB} cells treated or not treated with Dox revealed that, at both euchromatin and heterochromatin, the flap-hybridizing donor ODN.as consistently yielded a more even distribution between HDR and NHEJ events when compared to its ODN.s counterpart (**Figures 6C** and **6D**). These data suggest that base pairing assists in the engagement of flap-annealing ODNs with the RGN-cleaved target site dampening the contribution of the NHEJ pathway to the repair of the underlying site-specific DSBs. Importantly, when comparing ODN-based gene editing endpoints at euchromatin versus heterochromatin, these and follow-up ODN.as dose-response experiments were in agreement with the previous experiments using IDLV and plasmid donor DNA (**Figure 6E**). In particular, the frequencies of HDR and NHEJ were more comparable at heterochromatin than at euchromatin independently of ODN.as concentrations (**Figures 6F**, top graph). As a result, when target DNA sequences transit from an euchromatic to an heterochromatic state, there is a shift towards an increase in the preponderance of HDR over NHEJ (**Figure 6F**, bottom graph).

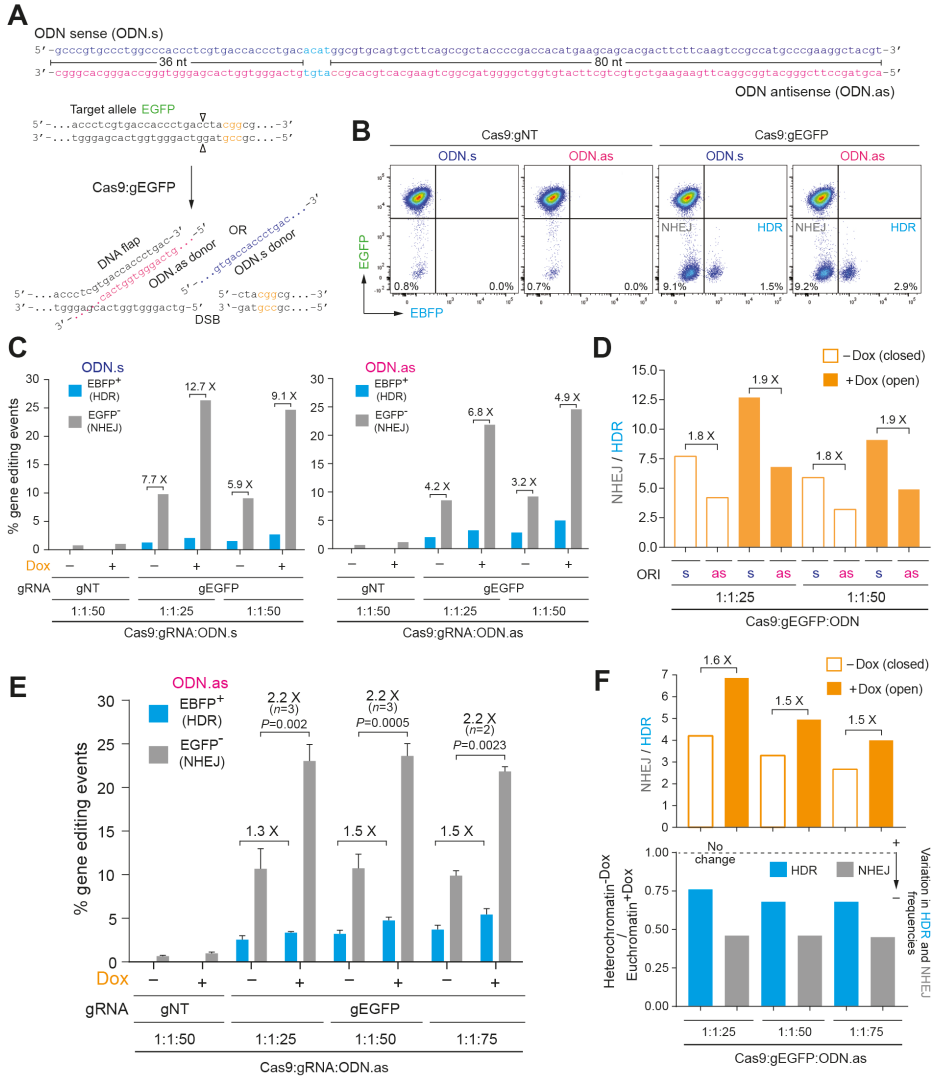


Figure 6. Gene editing endpoints at euchromatin versus heterochromatin after ODN donor delivery in HEK.EGFP^{TetO,KRAB} cells. **(A)** Schematics of ODN design and target site before and after RGN engagement. The RGN complex Cas9:gEGFP is presumed to generate a 3'-ended DNA flap complementary and non-complementary to ODN.as and ODN.s, respectively. HDR-based gene editing with ODN.s and ODN.as donors should result in EGFP-to-EBFP conversion. *Open arrowheads*, position of the DSB induced by Cas9:gEGFP. *Orange triplet*, PAM. **(B)** Probing HDR-based gene editing with sense and antisense ODNs. HEK.EGFP^{TetO,KRAB} cells were transfected with ODN.s or with ODN.as each mixed with expression plasmids coding for either non-cutting Cas9:gNT or cutting Cas9:gEGFP complexes. HDR and NHEJ quantification in HEK.EGFP^{TetO,KRAB} cells was assessed by EBFP- and EGFP-directed flow cytometry, respectively. **(C)** Testing the impact of chromatin structure on HDR-based gene editing with sense and antisense ODNs. HEK.EGFP^{TetO,KRAB} cells, incubated (+) or not incubated (-) with Dox, were exposed to the indicated experimental conditions. The frequencies of HDR and NHEJ were assessed by dual-color flow cytometry. **(D)** Relative participation of HDR and NHEJ pathways during the repair of euchromatic versus heterochromatic DSBs with ODNs with different polarities. Data of panel **C** displayed as the ratios between the frequencies of

HDR during heterochromatin repair

NHEJ and HDR in HEK.EGFP^{TetO.KRAB} cells treated and not treated with Dox. **(E)** ODN-based gene editing. Dual-color flow cytometric quantification of HDR and NHEJ frequencies in HEK.EGFP^{TetO.KRAB} cells. HEK.TLR^{TetO.KRAB} cells incubated (+) or not incubated (-) with Dox, were exposed to the indicated experimental conditions. Bars correspond to mean \pm s.d. of the indicated number (*n*) of independent experiments (biological replicates done in different days). **(F)** Relative participation of HDR and NHEJ pathways during ODN-mediated repair of DSBs taking place at heterochromatin versus euchromatin. Top graph, results of panel **E** shown as the ratios between the frequencies of NHEJ and HDR in HEK.EGFP^{TetO.KRAB} cells exposed or not exposed to Dox. Bottom graph, data of panel **E** presented as the variation in HDR and NHEJ events at heterochromatin versus euchromatin.

Taken our data together, we conclude that site-specific DSBs generated within euchromatin are mostly repaired through mutagenic NHEJ in detriment of error-free HDR. However, if the site-specific DSBs are made within heterochromatin instead, there is a more balanced participation of both cellular machineries in the repair of site-specific DNA lesions (**Figure 7**). Albeit varying in degree, this chromatin structure-dependent shift in the relationship between NHEJ and HDR takes place regardless of whether the donor DNA is presented in the context of IDLV genomes, recombinant plasmids or single-stranded ODNs, which together, makeup the most commonly used sources of exogenous genetic information.

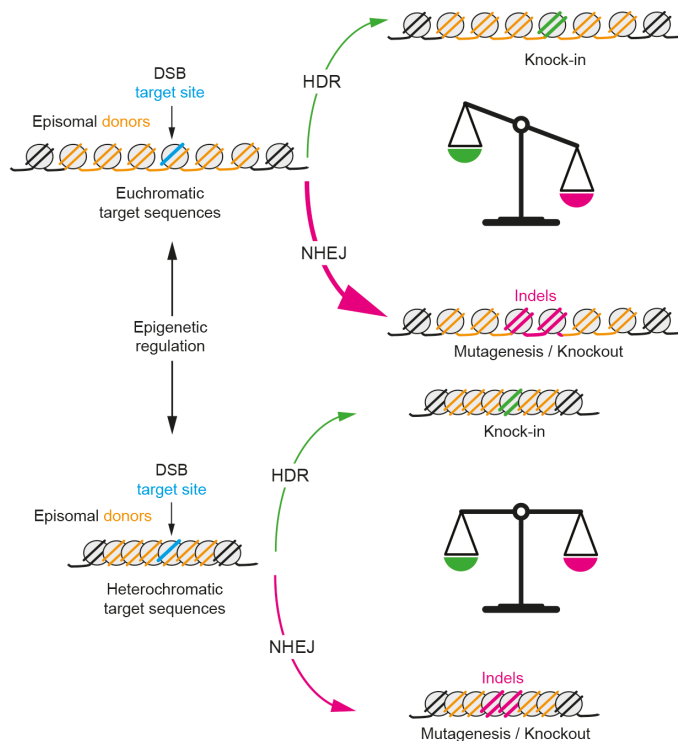


Figure 7. Summarizing illustration on the role of the chromatin structure on gene editing outcomes. The thickness of the curved arrows represents the relative contribution of homology-directed repair (HDR) and non-homologous end-joining (NHEJ) to gene editing endpoints at euchromatin versus heterochromatin.

Discussion

HDR-based genome editing is crucial for numerous research applications, including modelling, screening or correcting genotypes underlying human disorders in stem and/or progenitor cells. Crucially, accurate HDR takes place much less frequently than mutagenic NHEJ.^{3,4} Thus, identifying the biological parameters governing this strong DNA repair bias has both scientific and practical relevance. In this study, we have investigated the outcome of the interaction between the molecular tools necessary for HDR-based gene editing and the chromatin structure of target sequences. In particular, we assessed RGN-induced gene editing endpoints established after the engagement of donors of viral, non-viral and synthetic origins with isogenic target sequences located either in euchromatin or heterochromatin. We found that the relative proportions of gene editing endpoints resulting from mutagenic NHEJ and precise HDR events depend to a significant degree on the higher-order chromatin conformation of target sequences with a shift occurring towards HDR events at heterochromatin (**Figure 7**). This bias can vary in its extent, such as when using ssODNs with different polarities (~2-fold; **Figures 6C** and **6D**), but takes place independently of the type of episomal donor DNA utilized.

These findings suggest that HDR-based gene editing can be impacted by the epigenomic landscape of specific cell types as well as by the dynamic and epigenetically regulated chromatin changes underlying organismal development and cellular differentiation stages. Indeed, our experimental results support the hypothesis that the chromatin environment contributes to the well-known differential susceptibility of genomic sequences to gene editing interventions. Hence, the chromatin context of the target sequence should be taken into account whenever considering applying HDR-based gene editing procedures.

There is a paucity of knowledge about the repair mechanisms of DSBs located within different chromatin contexts in mammalian cells. In recent years, however, the classical view that heterochromatin simply poses a barrier to the DNA damage response (DDR) is changing into one in which heterochromatin and heterochromatin-associated proteins are active participants in it.²² For instance, SENP7 interacts with KAP-1 via HP1 α resulting in the deSUMOylation of KAP-1.²³ The removal of this post-translational modification from KAP-1 promotes the transient release of the co-repressors CHD3 and SETDB1 from chromatin, which in turn, creates a cellular milieu favorable for HDR-mediated DSB repair.²³ A similar milieu is conferred by the MRN-dependent recruitment of the histone acetyltransferase Trrap-Tip60 to



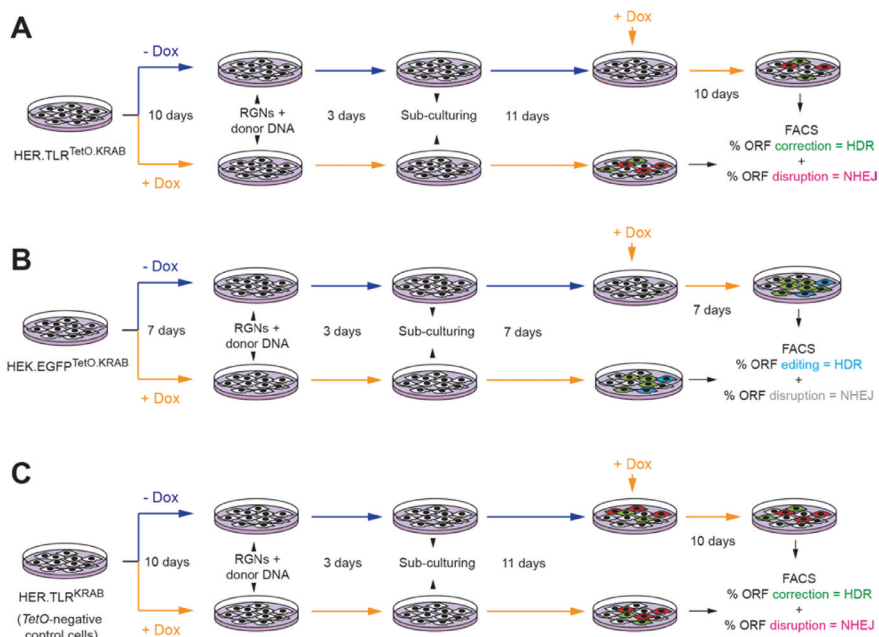
heterochromatic DSBs.²⁴ It has also been shown that HP1 α is transiently mobilized to both euchromatic and heterochromatic DSBs via an interaction with p150CAF-1, resulting in its higher accumulation at the latter lesions.²⁵ Interestingly, in HP1 α knockdown cells, in contrast to the buildup of the NHEJ factor XRCC4 at laser-induced DNA lesions, there is a markedly reduction of the HDR factors RAD51 and BRCA1 at these lesions.²⁵ Subsequent experiments, based on exposing cells to the restriction enzyme AsiSI, provided additional support for the participation of heterochromatin-resident HP1 proteins in associating BRCA1 with DSBs and facilitating HDR.²⁶

Recent experiments are also starting to shed light on the relationship between different cell cycle stages and DNA repair pathways at heterochromatic domains in mammalian cells. Study showed that DSBs created within pericentric heterochromatin during G1 remain stationary and are repaired through NHEJ, whilst in S or G2, these DSBs relocate to the periphery of the heterochromatic domain and, once there, become substrates for RAD51/BRCA2-dependent HDR.²⁷ This heterochromatic DSB migration to euchromatic regions might favor the finalization of proper HDR with sister chromatid or homologous chromosome sequences in detriment of ectopic HDR with repetitive DNA, common in heterochromatic regions. Remarkably, DSBs located within centromeric heterochromatin, recruit not only the NHEJ marker protein Ku80 but also the HDR factors RPA and RAD51 throughout the cell cycle with an enhancement observed during G2.²⁷

Collectively, these data provide compelling evidence for an active role of HDR during heterochromatic DSB repair involving an intricate interplay between histone marks (e.g. H3K9me3), chromatin remodeling factors (e.g. HP1 isoforms, CHD3, Trap-Tip60 and KAP-1) and DNA repair proteins (e.g. BRCA1, RPA and RAD51). It is worth mentioning, however, that for the most part, these experiments have relied on generating supra-physiological amounts of different types of DSBs throughout the genome either by ionizing radiation, laser micro-irradiation or restriction enzyme exposure. Moreover, the relative proportions between HDR and NHEJ events at sequences with distinct chromatin states in individual test cell populations were not investigated. Finally, although certain DDR processes seem to be specific for repairing heterochromatic DSBs, e.g., ATM-mediated phosphorylation of KAP-1,²⁸ some others appear to lack this specificity, e.g., p150CAF-1-mediated recruitment of HP1 α to DSBs.²⁵ It should thus be very instructive investigating which DDR components and mechanisms are specific to heterochromatin, euchromatin or shared by both compartments.

Concluding, in the present study, we have implemented cellular assays based on epigenetically regulated genetic reporters, donor DNA templates and RGNs for the simultaneous quantification of HDR and NHEJ events at single target sequences

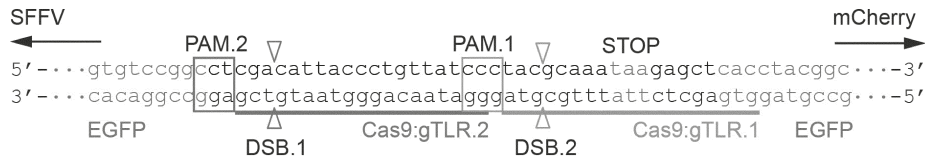
subjected to distinct chromatin conformations. The resulting data expand the aforementioned findings by providing direct experimental evidence for a role of the higher-order chromatin structure on the differential regulation of the two major DNA repair pathways in mammalian cells. The recruitment of DDR factors and DNA recombination substrates into a well-defined genetic and epigenetic environment offered by these live-cell tracking systems should aid detailed investigations into the mechanisms of DDR under different chromatin contexts as well as their interplay with other cellular mechanisms and DNA metabolic processes such as replication. Finally, as illustrated in the current study through experiments testing viral, non-viral and synthetic donors, this epigenetically-regulated experimental systems should also serve for assessing in cellula the impact of chromatin on novel gene editing protocols involving, amongst others, donor DNA substrates from different origins or with different structures and compositions, NHEJ-inhibiting reagents,^{29,30} and unexploited programmable nuclease systems.^{31,32}



HDR
during
hetero
DSB
repair

Supplementary Figure S1. Schematic representation of the experimental settings used in the current study. The tTR-KRAB-expressing cells HER.TLR^{TetO}.KRAB **(A)** and HEK.EGFP^{TetO}.KRAB **(B)** contain the Dox-regulated *TLR^{TetO}*⁹ and *EGFP^{TetO}*³³ constructs, respectively. These reporter cells, containing target sequences in a heterochromatic (-Dox) or euchromatic (+Dox) state, are transiently transfected with different combinations of gene editing tools consisting of RGNs and donor DNA templates. After the generation of site-specific DSBs and the ensuing modification of target DNA sequences in cells subjected to both experimental settings (i.e. -Dox and +Dox), target gene expression is activated to quantifying by flow cytometry

the frequencies of gene editing events resulting from the engagement of HDR and NHEJ pathways. The tTR-KRAB-expressing HER.TLR^{KRAB} reporter cells (**C**) have the Dox-insensitive TLR construct ¹¹ and were used as an isogenic control cellular system.



Supplementary Figure S2. Target sites of RGN complexes in the *TLR* construct. The target sequences for the RGN complexes Cas9:gTLR.1 and Cas9:gTLR.2 are indicated by horizontal lines linked to *open boxes* (PAM elements). The positions of the DSBs generated by each RGN are marked (*vertical open arrowheads*). STOP, nonsense codon located within the *TLR* ORF.

Supplementary Table S1. Oligonucleotide pairs to generate the gRNA expression constructs expressing gTLR.1, gTLR.2, gNT and gEGFP

Plasmids	Oligonucleotide pairs (5'- 3')
Z42_pgTLR.1	5'-ACCGGTGAGCTCTTATTTGCGTA-3' 5'-AAACTACGCAAATAAGAGCTCAC-3'
Z44_pTLR.2	5'-ACCGGATAACAGGGTAATGTCG-3 5'-AAACCGACATTACCCTGTTATCC-3'
AM51_pgNT	5'-ACCGGTGAGCTCTTATTTGCGTAGCTAGCTGAC-3 5'-AAACGTCAGCTAGCTACGCAAATAAGAGCTCAC-3'
AX03_pgEGFP	5'-ACCGCTCGTGACCACCCTGACCTA-3' 5'-AAACTAGGTCAGGGTGGTCACGAG-3'

Supplementary Table S2. Experimental scheme corresponding to **Figure 2 (Protocol A)**

DONOR: IDLV ^d	3.25 × 10 ⁵ HER.TLR ^{TetO,KRAB} cells per well of 24-well plates (500 µl medium per well with or without Dox)			
	PEI (1mg/ml) 5.8 µl per well; Ratio DNA / PEI equivalents = 6			
Reagents	Cas9	gNT (Ctrl)	gTLR.1	Total (ng)
Construct length (bp)	9551	3056	3046	
DNA per well (ng)	1327	423		1750
	1327		423	1750
	1327			1750

Note 1: One day after transfecting plasmids expressing Cas9 and gTLR.1, IDLV^d particles were added at an MOI of 4, 8, 12 and 16 VP/cell; **Note 2:** One day after transfecting plasmids expressing Cas9 and gNT, IDLV^d particles were added at an MOIs of 8 VP/cell.

Supplementary Table S3. Experimental scheme corresponding to **Figure 3A (Protocol A)**

DONOR: IDLV ^d	3.25 × 10 ⁵ HER.TLR ^{TetO.KRAB} cells per well of 24-well plates (500 µl medium per well with or without Dox)				
	PEI (1mg/ml) 5.8 µl per well; Ratio DNA / PEI equivalents = 6				
Reagents	Cas9	gNT (Ctrl)	gTLR.1	gTLR.2	Total (ng)
Construct length (bp)	9551	3056	3046	3046	
DNA per well (ng)	1327	423			1750
	1327		423		1750
	1327			423	1750

Note: One day after transfecting the indicated plasmids, IDLV^d particles were added at an MOI of 8 VP/cell.

Supplementary Table S4. Experimental scheme corresponding to **Figure 3B (Protocol B)**

DONOR: IDLV ^d	3.25 × 10 ⁵ HER.TLR ^{TetO.KRAB} cells per well of 24-well plates (500 µl medium per well with or without Dox)			
	PEI (1mg/ml) 9.6 µl per well; Ratio DNA / PEI equivalents = 10			
Reagents	Cas9	gNT (Ctrl)	gTLR.1	Total (ng)
Construct length (bp)	9551	3056	3046	
DNA per well (ng)	1327	423		1750
	1327		423	1750
	1327			1750

Note: One day after transfection of the indicated plasmids, IDLV^d particles were added at an MOI of 8 VP/cell.

Supplementary Table S5. Experimental scheme corresponding to **Figure 3E (Protocol A)**

DONOR: Plasmid ^d	3.25 × 10 ⁵ HER.TLR ^{TetO.KRAB} cells per well of 24-well plates (500 µl medium per well with or without Dox)					
	PEI (1mg/ml) 5.8 µl per well; Ratio DNA / PEI equivalents = 6					
Reagents	Cas9	gNT (Ctrl)	gTLR.1	gTLR.	Plasmid ^d	Total (ng)
Construct length (bp)	9551	3056	3046	3046	6194	
DNA per well (ng)	890	284			577	1751
	890		284		577	1751
	890			284	577	1751



Supplementary Table S6. Experimental scheme corresponding to **Figure 3F (Protocol B)**

DONOR: Plasmid ^d	3.25 × 10 ⁵ HER.TLR ^{TetO.KRAB} cells per well of 24-well plates (500 µl medium per well with or without Dox)					
	PEI (1mg/ml) 9.6 µl per well; Ratio DNA / PEI equivalents = 10					
Reagents	Cas9	gNT (Ctrl)	gTLR.1	gTLR.2	Plasmid ^d	Total
Construct length (bp)	9551	3056	3046	3046	6194	(ng)
DNA per well (ng)	890	284			577	1751
	890		284		577	1751
	890			284	577	1751

Supplementary Table S7. Experimental scheme corresponding to **Figure 5**

DONOR: pTHG.Donor (Exp.1)	2.0 × 10 ⁵ HEK.EGFP ^{TetO.KRAB} cells per well of 24-well plates (500 µl medium per well with or without Dox)				
	PEI (1mg/ml) 6.2 µl per well; Ratio DNA / PEI equivalents = 9				
Reagents	eCas9	gEGFP	gNT (Ctrl)	pTHG.Donor	Total
Construct length (bp)	9360	3046	3056	3561	(ng)
DNA per well (ng)	733	238		279	1250
	733		238	279	1250
DONOR: pTHG.Donor (Exp.2)	2.0 × 10 ⁵ HEK.EGFP ^{TetO.KRAB} cells per well of 24-well plates (500 µl medium per well with or without Dox)				
	PEI (1mg/ml) 6.2 µl per well; Ratio DNA / PEI equivalents = 9				
Reagents	eCas9.2	gEGFP	gNT (Ctrl)	pTHG.Donor	Total
Construct length (bp)	9403	3046	3056	3561	(ng)
DNA per well (ng)	733	238		279	1250
	733		238	279	1250

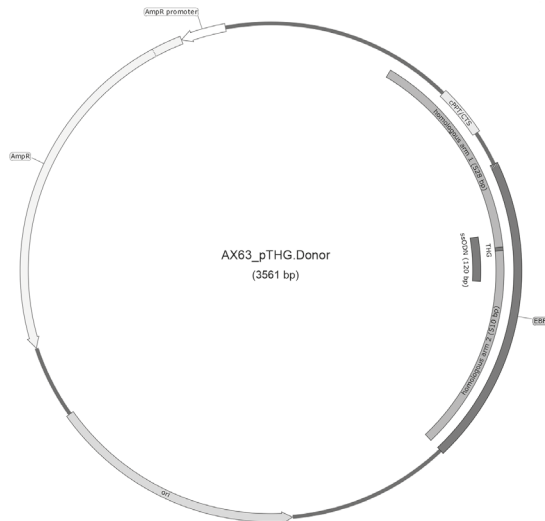
Supplementary Table S8. Experimental scheme corresponding to **Figure 6C**

DONOR: ODN.s / ODN.as	2.5 × 10 ⁵ HEK.EGFP ^{TetO.KRAB} cells per well of 24-well plates (500 µl medium per well with or without Dox)						
	PEI (1mg/ml) 6.2 µl per well; Ratio DNA / PEI equivalents = 9						
Reagents	Cas9	gNT (Ctrl)	gEGFP	ODN.s	ODN.as	Total	Molar ratios
Construct length (bp)	9551	3056	3046	120	120	(ng)	
DNA per well (ng)	642	205		403		1250	1:1:50
	766		244	240		1250	1:1:25
	642		205	403		1250	1:1:50
	642	205			403	1250	1:1:50
	766		244		240	1250	1:1:25
	642		205		403	1250	1:1:50

Supplementary Table S9. Experimental scheme corresponding to Figure 6E

DONOR:	2.5 × 10 ⁵ HEK.EGFP ^{TetO.KRAB} cells per well of 24-well plates (500 µl medium per well with or without Dox)					
ODN.s / ODN.as	PEI (1mg/ml): 6.2 µl per well; Ratio DNA / PEI equivalents = 9					
Reagents	Cas9	gNT (Ctrl)	gEGFP	ODN.as	Total	Molar ratios
Construct length (bp)	9551	3056	3046	120	(ng)	
DNA per well (ng)	642	205		403	1250	1:1:50
	766		244	240	1250	1:1:25
	642		205	403	1250	1:1:50
	553		176	521	1250	1:1:75

Supplementary Notes



>AX63_pTHG.Donor

GGAAACAGCTATGACCATGATTACGCCAAGCTCGAAATTACCCCTCACTAAAGGGAACAAAGCTGGTACGAGGACAGGCTGGAGC-CATGGGCATGGCTACTCAAGCTGATTTGATGGAGTTGGACATGGCCATGGCTGGTGACCACTCGTGGGAATGCCTTCGAATTCAG-CACCTGCACATGGGACGTCGACCTGAGGTAATTATAACCCGGGCCCTATATGGATCCAATTGCAATGATCATATGACAGATCGC-CGCGATCGATATCAGCGCTTTAAATTTGCGCATGCTAGCTATAGTTCTAGAGCCTCTGCTAACCATGTTTCATGCCTTCTTTCTTCTA-CAGCTCCTGGGCAACGTGCTGTTATTGTGCTGTCTCATTTTTGGCAAAGAATTAATTTAATTAATCTCGACGGTATCGGTTA-ACTTTTAAAGAAAAGGGGGGATTGGGGGTACAGTGCAGGGGAAAGAATAGTAGACATAATAGCAACAGACATACAAATTTAAAGAAT-TACAAAAACAAATTACAAAAATTCAAATTTTATCGATCACGAGACTAGCCTCGAGGTTTAAACTACGGGATCCAGGCCTAAGCTTACG-CGTCTAGCGCTACCGTCCACCATGGTGAAGGCGAGGAGCTGTTACCGGGGTGGTCCCATCCTGGTCGAGCTGGAC-GGCGACGTAAACGCCACAAGTTTCAGCGTGTCCGGCAGGGGCGAGGGCGATGCCACCTACGGCAAGCTGACCCCTGAAGTTTCATCTG-CACCACCGGAAGCTGCCGTGCCCTGGCCACCCTCGTGACCACCCTG**ACACATGGCGTGCAGTGCCTCAGCCGCTACCCCGAC-CACATGAAGCAGCAGACTTCTCAAGTCCGCCATGCCGAAGGCTACGTCAGGAGCGCACCATCTTCTTCAAGGACGACGG-CAACTACAAGACCCGCGCCGAGGTGAAGTTCGAGGGCGACACCCTGGTGAACCGCATCGAGCTGAAGGGCATCGACTCAAGGAG-GACGGCAACATCCTGGGGCACAAGCTGGAGTACAACATAACAGCCACAACGTCATATCATGGCCGACAAGCAGAAGAAGCGG-CATCAAGTGAACTTCAAGATCCGCCACAACATCGAGGACGGCAGCGTGCAGCTCGCCGACCACTACCAGCAGAACACCCCATC-GGCGACGGCCCCGTGCTGCTGCCCGACAACCACTACCTGAGCACCCAGTCCGCCCTGAGCAAAGACCCCAACGAGAAGCGGAT-CACATGGTCTGCTGGAGTTCGTGACCGCCCGGGATCACTCTCGGCATGGACGAGCTGTACAGAGCTCGAGAAGTACTAGTG-GCCACGTGGGCCGTGCACCTTAAGCTTTTAAATAAGGAGGAATAACATATGACCATGATTACGCCAAGCTCCAATTCGCCCTATAGT-GAGTCGTATTACAATTCAGTGGCCGTGTTTTACTATGCGGTGTGAAATACCCGCACAGATGCGTAAGGAGAAAATACCGCATCAGG-**



CGCTCTCCGCTTCTCGCTACTGACTCGCTCGCTCGGCTCGGCTCGGCTCGGCGAGCGGTATCAGCTCACTCAAAGCGGTA-
 ATACGGTTATCCACAGAATCAGGGGATAACGCAGGAAAGAACATGTGAGCAAAAGGCCAGCAAAAGGCCAGGAACCGTAAAAAG-
 GCCGCGTTGCTGGCGTTTTTCCATAGGCTCCGCCCCCTGACGAGCATCACAAAATCGACGCTCAAGTCAGAGGTGGCGAAAC-
 CCGACAGGACTATAAAGATACCAGGCGTTTCCCCCTGGAAGCTCCCTCGTGCCTCTCTGTTCCGACCTGCCGCTTACCGGA-
 TACCTGTCCGCTTTCTCCCTTCCGGAAGCGTGGCGCTTTCATAGCTCAGCTGTAGGTATCTCAGTTCCGTTGATGGTCTGCTC-
 CAAGCTGGGCTGTGTGCACGAACCCCGCTTCAAGCCGACCGCTGCGCCTTATCCGGTAACTATCGTCTTGAGTCCAACCCGGTAAAG-
 ACACGACTTATCGCCACTGGCAGCAGCCACTGGTAACAGGATTAGCAGAGCGAGGTATGTAGGCGGTGCTACAGAGTTCTTGAAGT-
 GGTGGCCTAACTACGGCTACTAGAAAGACAGTATTTGGTATCTGCGCTCTGCTGAAGCCAGTTACCTTCGAAAAAGAGTTGG-
 TAGCTCTTGATCCGCAACAACACCAGCTGGTAGCGTGGTTTTTTTTGTTTGAAGCAGCAGATTACGCCAGAAAAAAGGATCT-
 CAAGAAGATCCTTTGATCTTTTCTACGGGGTCTGACGCTCAGTGGAACGAAAACTCACGTTAAGGGATTTTGGTCATGAGATTAT-
 CAAAAAGGATCTTACCTAGATCCTTTTAAATAAAAATGAAGTTTTAAATCAATCTAAAGTATATATGAGTAAACTTGGTCTGACAGT-
 TACCAATGCTTAATCAGTGAGGCACCTATCTCAGCGATCTGTCTATTTTCATCCATAGTTGCCTGACTCCCGCTCGTGATAGATAAC-
 TACGATACGGGAGGGCTTACCATCTGCCCCAGTGTGCAATGATACCGCGAGACCCACGCTCACCGGCTCCAGATTTATCAGAAATA-
 AACCGCCAGCCGGAAGGGCCGAGCGCAGAAGTGGTCTGCAACTTTATCCGCTCCATCCAGTCTATTAATTTGTCCGGGAAGCTA-
 GAGTAAGTAGTTCGCCAGTTAATAGTTTGCACAACGTTGTTGCCATTGCTGCAGGCATCGTGGTGCACGCTCGTCGTTTGGTATG-
 GCTTCATTCAGCTCCGTTCCCAACGATCAAGGCGAGTTACATGATCCCCATGTTGTGCAAAAAAGCGGTTAGTCTCTCGGTCCTC-
 CGATCGTTGTGAGAAGTAAAGTTGGCCGAGTGTATCACTCATGTTATGGCAGCACTGCATAATCTCTTACTGTATGCCATCCGTA-
 AGATGCTTTTCTGTGACTGGTGAAGTACTCAACCAAGTCACTGAGAAATAGTGTATGCGGCGACCGAGTTGCTCTTGGCCGCGTCAA-
 CACGGGATAATACCGCCACATAGCAGAACTTTAAAGTGTCTCATCTTGGAAAACGTTCTTCCGGGGCGAAAACTCTCAAGGATCT-
 TACCGCTGTTGAGATCCAGTTCGATGTAACCCACTCGTGCACCCAACTGATCTTCCAGCATCTTTTACTTTCCACAGCGTTTCTGGGT-
 GAGCAAAAACAGGAAGGCAAAATGCCGCAAAAAGGGAATAAGGGCGACACGAAATGTTGAATACTCATACTTCTCTTTTCAATAT-
 TATTGAAGCATTTATCAGGGTATTGTCTCATGAGCGGATACATATTTGAATGTATTTAGAAAAATAACAAATAGGGGTTCCCGCGCA-
 CATTTCGCCGAAAAGTGCCACCTGACGTCTAAGAAACCATATTATCATGACATTAACCTATAAAAAATAGGCGTATCACGAGGCCCTTTC-
 GTCTCAAGAATT

Map and nucleotide sequence of pTHG.Donor for HDR-mediated editing of *EGFP* into *EBFP*. DNA sequences sharing identity to the target sequence in HEK.EGFP^{TetO.KRAB} cells are indicated in orange; AmpR, β -lactamase ampicillin resistance gene; ori, high-copy number ColE1 prokaryotic origin of replication; cPPT/CTS, central polypurine tract and central termination sequence of HIV-1. As reference, the nucleotide sequences corresponding to the EBFP fluorochrome (Thr-His-Gly) and the ssODNs are highlighted in bold and underlined, respectively.

Methods

Cells

The human embryonic retinoblasts HER.TLR^{TetO.KRAB} and their control *TetO*-negative counterparts HER.TLR^{KRAB}, were generated and cultured as detailed elsewhere.⁶ Likewise for the human embryonic kidney cells HEK.EGFP^{TetO.KRAB}.⁶ The HEK293T cells (American Type Culture Collection) used for the generation of IDLV⁴ preparations were maintained in Dulbecco's modified Eagle's medium (DMEM; Thermo Fisher Scientific) supplemented with 10% fetal bovine serum (FBS; Thermo Fisher Scientific). The cells used in this study were mycoplasma free and were kept at 37°C in a humidified-air 10% CO₂ atmosphere.

Recombinant DNA

The gRNA acceptor construct S7_pUC.U6.sgRNA.BveI-stuffer contains a human U6 RNA Pol III promoter and terminator sequence for gRNA expression.⁶ The gRNA expression plasmids; Z42_pgTLR.1, Z44_pgTLR.2, AM51_pgNT and AX03_pgEGFP were generated by ligating the annealed oligonucleotide pairs listed in **Supplementary Table S1** into BveI-digested S7_pUC.U6.sgRNA.BveI-stuffer. The plasmid hCas9 was used for expressing the *Streptococcus pyogenes* Cas9 nuclease (Addgene plasmid #41815).¹¹ The sequence and annotated map of construct AX63_pTHG.donor used for HDR-mediated editing of *EGFP* into *EBFP*, are shown in **Sup-**

plementary Notes. The Addgene plasmid #31475 pCVL SFFV d14 GFP,¹² herein named Plasmid^d, served as a source of donor DNA in the gene editing experiments performed on HER.TLR^{TetO.KRAB} and HER.TLR^{KRAB} cells. Plasmid^d is a lentiviral vector construct that harbours the TLR-targeting donor template *EGFPtrunc*.¹²

DNA transfections

The DNA transfections performed on cultures of HER.TLR^{TetO.KRAB} were initiated by adding 1 mg/ml of linear 25 kDa polyethyleneimine (PEI, Polysciences) to the different plasmid mixtures diluted in 50 μ l of 150 mM NaCl (**Supplementary Tables S2-S6**). These cell cultures were pre-incubated for 10 days in medium lacking or containing doxycycline (Dox) at a final concentration of 0.5 μ g/ml. An approximately 10-sec period of vigorous vortexing followed the addition of the PEI polycation to each of the DNA mixtures. Next, the DNA-PEI complexes were let to be formed for 15 min at room temperature after which they were directly added to the culture medium of the various target cells seeded one day before in wells of 24-well plates (Greiner Bio-One). The different transfection mixtures were substituted 6-8 hours later by regular culture medium with or without Dox. At 3 days post-transfection, the cells were sub-cultured every 3-4 days for a period of 10 days and the frequencies of EGFP- and mCherry-positive cells in the cultures containing Dox were determined by flow cytometry (**Supplementary Figure S1**). To activate transgene expression, the cultures initially lacking Dox were exposed to Dox (0.5 μ g/ml) for 10 days, after which the frequencies of EGFP- and mCherry-positive cells were also determined in these cultures by flow cytometry. The experimental design, transfection protocols and Dox regimens applied to *TetO*-negative HER.TLR^{KRAB} cells were the same as those applied to HER.TLR^{TetO.KRAB} cells (**Supplementary Figure S1**).

The DNA transfections carried out on cultures of HEK.EGFP^{TetO.KRAB} cells started by adding 1 mg/ml of PEI to the different plasmid mixtures diluted in 50 μ l of 150 mM NaCl (**Supplementary Tables S7-S9**). These cell cultures were pre-incubated for 7 days in medium lacking or supplemented with Dox at a final concentration of 0.2 μ g/ml. After the addition of PEI to the DNA solutions, an approximately 10-sec period of vigorous vortexing followed. Subsequently, the DNA-PEI complexes were assembled for 15 min at room temperature after which they were directly added to the culture medium of the various target cells that had been seeded one day before in wells of 24-well plates (Greiner Bio-One). The various transfection mixtures were replaced 6-8 hours later by regular culture medium with or without Dox. At 3 days post-transfection, the cells were sub-cultured every 3-4 days for a period of 7 days and the frequencies of EBFP-positive and EGFP-negative cells in the cultures containing Dox were determined by flow cytometry. To activate transgene expression, the cultures that initially had not received Dox were incubated in the presence of Dox (0.2 μ g/ml) for an additional 7-day period, after which the frequencies of EBFP-positive and EGFP-negative cells were also determined in these cultures by flow cytometry (**Supplementary Figure S1**).

IDLV production and titration

The assembly of IDLV^d particles was carried out by transient transfections of HEK293T cells



with lentiviral vector construct Plasmid^d,¹² together with packaging plasmid AM16_psPAX2. IN^{D116N},¹³ and vesicular stomatitis virus glycoprotein-G-pseudotyping construct pLP/VSVG (Thermo Fisher Scientific), as detailed previously.^{13,14} The protocols for the concentration and purification of IDLV^d particles released into the producer-cell culture medium were equally detailed elsewhere.^{13,14} Finally, the physical particle titers of the resulting IDLV^d stocks were determined by measuring the HIV-1 p24gag antigen with the aid of the RETRO-TEK HIV-1 p24 ELISA kit following the manufacturer's instructions (Gentaur Molecular Products).

Gene editing experiments with single-stranded ODNs

The 120 nucleotide-long single-stranded ODNs ODN.s (5'-GCCCGTGCCT-GGCCCACCCTCGTGACCACCCTGACACATGGCGTGCA GTGCT-T CAGCCGCTA CCCC GACCACATG AAGCAGC ACGACTTCT-TCAAGTCCGCCATGCCCGAAGGCTACGT-3') and ODN.as (5'-ACGTAGCCTTCGGGCATGGCGGACTTGAAGAAGTCGTGCTGCTTCATGTGGTCG-GGGTAGCGGCTGAAGCACTGCACGCCATGTGTCAGGGTGGTCACGAGGGTGGGC-CAGGGCACGGGC-3') were custom synthesized and HPLC-purified (Eurofins Scientific). These ODNs were reconstituted in a solution of 10 mM Tris-Cl and 1 mM EDTA (pH 8.0) to a concentration of 100 pmol/μl. A fifty-fold dilution of this stock was divided in aliquots and stored at -20°C prior to transfection. The ODNs were transfected together with RGN-encoding plasmids into HEK.EGFP^{TetO.KRAB} cells cultured in the absence or in the presence of Dox (0.2 μg/ml) using the previously described PEI-based protocol and the DNA mixtures detailed in **Supplementary Tables S8 and S9**.

Flow cytometry

The measurements of EGFP-positive, EGFP-negative, EBFP-positive and mCherry-positive cells were performed using a BD LSR II flow cytometer (BD Biosciences). The data were analysed with the support of FlowJo 10.1 software (Tree Star) or BD FACSDiva 6.1.3 software (BD Biosciences). Mock-transfected cells served for establishing background fluorescence thresholds. At least 40,000 viable single cells were analysed per sample.

Statistical analysis

The comparison of the indicated data sets resulting from independent experiments (biological replicates done in different days) were analysed by applying two-tailed Student's *t*-tests ($P < 0.05$ considered significant). The GraphPad Prism 6 software package was used for this analysis.

Acknowledgments

The authors thank Rob Hoeben and Ignazio Maggio (Leiden University Medical Center, Departments of Molecular Cell Biology and Pediatrics, respectively) for their critical reading of the manuscript. This work was partially supported by the Dutch Prinses Beatrix Spierfonds (W.OR11-18) and ProQR Therapeutics (Leiden, the Netherlands). X.C. holds a Ph.D. research grant from the China Scholarship Council-Leiden University Joint Scholarship Programme.

Conflict of interest statement. None declared.

Reference

1. Kim H, Kim J-S. A guide to genome engineering with programmable nucleases. *Nat Rev Genet.* 2014;15:321-334. DOI: 10.1038/nrg3686
2. Maggio I, Goncalves MA. Genome editing at the crossroads of delivery, specificity, and fidelity. *Trends Biotechnol.* 2015;33:280-291. DOI: 10.1016/j.tibtech.2015.02.011
3. Chang HHY, Pannunzio NR, Adachi N et al. Non-homologous DNA end joining and alternative pathways to double-strand break repair. *Nat Rev Mol Cell Biol.* 2017;18:495-506. DOI: 10.1038/nrm.2017.48
4. Heyer WD. Regulation of recombination and genomic maintenance. *Cold Spring Harb Perspect Biol.* 2015;7:a016501. DOI: 10.1101/cshperspect.a016501
5. Kouzarides T. Chromatin modifications and their function. *Cell* 2007;128:693-705. DOI: 10.1016/j.cell.2007.02.005
6. Chen X, Rinsma M, Janssen JM et al. Probing the impact of chromatin conformation on genome editing tools. *Nucleic Acids Res.* 2016;44:6482-6492. DOI: 10.1093/nar/gkw524
7. Daer RM, Cutts JP, Brafman DA et al. The Impact of Chromatin Dynamics on Cas9-Mediated Genome Editing in Human Cells. *ACS Synth Biol.* 2017;6:428-438. DOI: 10.1021/acssynbio.5b00299
8. Doudna JA, Charpentier E. The new frontier of genome engineering with CRISPR-Cas9. *Science* 2014;346. DOI: 10.1126/science.1258096
9. Wanisch K, Yanez-Munoz RJ. Integration-deficient lentiviral vectors: a slow coming of age. *Mol Ther.* 2009;17:1316-1332. DOI: 10.1038/mt.2009.122
10. Anders C, Niewoehner O, Duerst A et al. Structural basis of PAM-dependent target DNA recognition by the Cas9 endonuclease. *Nature* 2014;513:569-573. DOI: 10.1038/nature13579
11. Mali P, Yang L, Esvelt KM et al. RNA-Guided Human Genome Engineering via Cas9. *Science* 2013;339:823-826. DOI: 10.1126/science.1232033
12. Certo MT, Ryu BY, Annis JE et al. Tracking genome engineering outcome at individual DNA breakpoints. *Nat Methods.* 2011;8:671-676. DOI: 10.1038/nmeth.1648
13. Pelascini LPL, Janssen JM, Goncalves MAFV. Histone Deacetylase Inhibition Activates Transgene Expression from Integration-Defective Lentiviral Vectors in Dividing and Non-Dividing Cells. *Hum Gene Ther.* 2013;24:78-96. DOI: 10.1089/hum.2012.069
14. Pelascini LP, Goncalves MA. Lentiviral vectors encoding zinc-finger nucleases specific for the model target locus HPRT1. *Methods Mol Biol.* 2014;1114:181-199. DOI: 10.1007/978-1-62703-761-7_12
15. Urrutia R. KRAB-containing zinc-finger repressor proteins. *Genome Biol.* 2003;4:231. DOI: 10.1186/gb-2003-4-10-231
16. Iyengar S, Farnham PJ. KAP1 Protein: An Enigmatic Master Regulator of the Genome. *J Biol Chem.* 2011;286:26267-26276. DOI: 10.1074/jbc.R111.252569
17. Groner AC, Meylan S, Ciuffi A et al. KRAB-Zinc Finger Proteins and KAP1 Can Mediate Long-Range Transcriptional Repression through Heterochromatin Spreading. *PLoS Genet.*



2010;6:e1000869. DOI: 10.1371/journal.pgen.1000869

18. Kucsu C, Arslan S, Singh R et al. Genome-wide analysis reveals characteristics of off-target sites bound by the Cas9 endonuclease. *Nat Biotech.* 2014;32:677-683. DOI: 10.1038/nbt.2916

19. Wu X, Scott DA, Kriz AJ et al. Genome-wide binding of the CRISPR endonuclease Cas9 in mammalian cells. *Nat Biotech.* 2014;32:670-676. DOI: 10.1038/nbt.2889

20. O'Geen H, Henry IM, Bhakta MS et al. A genome-wide analysis of Cas9 binding specificity using ChIP-seq and targeted sequence capture. *Nucleic Acids Res.* 2015;43:3389-3404. DOI: 10.1093/nar/gkv137

21. Richardson CD, Ray GJ, DeWitt MA et al. Enhancing homology-directed genome editing by catalytically active and inactive CRISPR-Cas9 using asymmetric donor DNA. *Nat Biotech.* 2016;34:339-344. DOI: 10.1038/nbt.3481

22. Watts FZ. Repair of DNA Double-Strand Breaks in Heterochromatin. *Biomolecules* 2016;6:47. DOI: 10.1042/BST20110631

23. Garvin AJ, Densham RM, Blair-Reid SA et al. The deSUMOylase SENP7 promotes chromatin relaxation for homologous recombination DNA repair. *EMBO Rep.* 2013;14:975-983. DOI: 10.1038/embor.2013.141

24. Murr R, Loizou JI, Yang YG et al. Histone acetylation by Trrap-Tip60 modulates loading of repair proteins and repair of DNA double-strand breaks. *Nat Cell Biol.* 2006;8:91-99. DOI: 10.1038/ncb1343

25. Baldeyron C, Soria G, Roche D et al. HP1alpha recruitment to DNA damage by p150CAF-1 promotes homologous recombination repair. *J Cell Biol.* 2011;193:81-95. DOI: 10.1083/jcb.201101030

26. Lee YH, Kuo CY, Stark JM et al. HP1 promotes tumor suppressor BRCA1 functions during the DNA damage response. *Nucleic Acids Res.* 2013;41:5784-5798. DOI: 10.1093/nar/gkt231

27. Tsouroula K, Furst A, Rogier M et al. Temporal and Spatial Uncoupling of DNA Double Strand Break Repair Pathways within Mammalian Heterochromatin. *Mol Cell.* 2016;63:293-305. DOI: 10.1016/j.molcel.2016.06.002

28. Goodarzi AA, Noon AT, Deckbar D et al. ATM signaling facilitates repair of DNA double-strand breaks associated with heterochromatin. *Mol Cell.* 2008;31:167-177. DOI: 10.1016/j.molcel.2008.05.017

29. Chu VT, Weber T, Wefers B et al. Increasing the efficiency of homology-directed repair for CRISPR-Cas9-induced precise gene editing in mammalian cells. *Nat Biotech.* 2015;33:543-548. DOI: 10.1038/nbt.3198

30. Robert F, Barbeau M, Ethier S et al. Pharmacological inhibition of DNA-PK stimulates Cas9-mediated genome editing. *Genome Med.* 2015;7:93. DOI: 10.1186/s13073-015-0215-6

31. Chylinski K, Makarova KS, Charpentier E et al. Classification and evolution of type II CRISPR-Cas systems. *Nucleic Acids Res.* 2014;42:6091-6105. DOI: 10.1093/nar/gku241

32. Burstein D, Harrington LB, Strutt SC et al. New CRISPR-Cas systems from uncultivated microbes. *Nature* 2017;542:237-241. DOI: 10.1038/nature21059